TOXICOLOGICAL SCIENCES, 166(1), 2018, 51–64

doi: 10.1093/toxsci/kfy183
Advance Access Publication Date: July 16, 2018
Research Article

In Vitro Transformation of Human Bronchial Epithelial Cells by Diesel Exhaust Particles: Gene Expression Profiling and Early Toxic Responses

Iselin Rynning,[*] Jiri Neca,[†] Kristyna Vrbova,[‡] Helena Libalova,[‡] Pavel Rossner Jr ,[‡] Jørn A. Holme,[§] Kristine B. Gützkow,[¶] Anani K. Johnny Afanou,[*] Yke J. Arnoldussen,[*] Eva Hruba,[†] Øivind Skare,[‖] Aage Haugen,[*] Jan Topinka,[‡] Miroslav Machala,[†] and Steen Mollerup[*,1]

[*]Section for Toxicology and Biological Work Environment, Department of Chemical and Biological Work Environment, National Institute of Occupational Health, N-0304 Oslo, Norway; [†]Department of Chemistry and Toxicology, Veterinary Research Institute, 621 00 Brno, Czech Republic; [‡]Department of Genetic Toxicology and Nanotoxicology, Institute of Experimental Medicine of the Czech Academy of Sciences, 142 20 Prague, Czech Republic; [§]Division of Infection Control, Environment and Health, Department of Air and Noise; and [¶]Division of Infection Control, Department of Molecular Biology, Norwegian Institute of Public Health, N-0304 Oslo, Norway; and [‖]Department of Occupational Medicine and Epidemiology, National Institute of Occupational Health, N-0304 Oslo, Norway

[1]To whom correspondence should be addressed at Section for Toxicology and Biological Work Environment, Department of Chemical and Biological Work Environment, National Institute of Occupational Health, PO Box 5330 Majorstuen, N-0304 Oslo, Norway. E-mail: steen.mollerup@stami.no.

ABSTRACT

Occupational exposure to diesel exhaust may cause lung cancer in humans. Mechanisms include DNA-damage and inflammatory responses. Here, the potential of NIST SRM2975 diesel exhaust particles (DEP) to transform human bronchial epithelial cells (HBEC3) *in vitro* was investigated. Long-term exposure of HBEC3 to DEP led to increased colony growth in soft agar. Several DEP-transformed cell lines were established and based on the expression of epithelial-to-mesenchymal-transition (EMT) marker genes, one of them (T2-HBEC3) was further characterized. T2-HBEC3 showed a mesenchymal/fibroblast-like morphology, reduced expression of *CDH1*, and induction of *CDH2* and *VIM*. T2-HBEC3 had reduced migration potential compared with HBEC3 and little invasion capacity. Gene expression profiling showed baseline differences between HBEC3 and T2-HBEC3 linked to lung carcinogenesis. Next, to assess differences in sensitivity to DEP between parental HBEC3 and T2-HBEC3, gene expression profiling was carried out after DEP short-term exposure. Results revealed changes in genes involved in metabolism of xenobiotics and lipids, as well as inflammation. HBEC3 displayed a higher steady state of *IL1B* gene expression and release of IL-1β compared with T2-HBEC3. HBEC3 and T2-HBEC3 showed similar susceptibility towards DEP-induced genotoxic effects. Liquid-chromatography-tandem-mass-spectrometry was used to measure secretion of eicosanoids. Generally, major prostaglandin species were released in higher concentrations from T2-HBEC3 than from HBEC3 and several analytes were altered after DEP-exposure. In conclusion, long-term exposure to DEP-transformed human bronchial epithelial cells *in vitro*. Differences between HBEC3 and T2-HBEC3 regarding baseline levels and DEP-induced changes of particularly *CYP1A1*, IL-1β, PGE_2, and $PGF_{2\alpha}$ may have implications for acute inflammation and carcinogenesis.

Key words: diesel exhaust particles; human bronchial epithelial cells; *in vitro* transformation; epithelial-to-mesenchymal transition; gene expression profiling; eicosanoid secretion.

The impact of particulate air pollution on human health is of major concern worldwide (Cohen *et al.*, 2005). Exposure to particulate matter from diesel engine exhaust (DEP) is a potential health hazard, especially in larger cities with extensive traffic pollution and in occupational settings where heavy-duty diesel engines are operated in enclosed areas (Benbrahim-Tallaa *et al.*, 2012). A link between exposure to diesel exhaust (DE) and increased risk of developing respiratory and cardiovascular diseases has been established (Pope *et al.*, 2002; Sydbom *et al.*, 2001). Based on studies in miners, exposure to DE has been classified as carcinogenic to humans (Benbrahim-Tallaa *et al.*, 2012).

The particulate phase of DE consists both of fine (<2.5 μm) and ultrafine (<0.1 μm) particles, that deposit mainly in the peripheral parts of the lung where they directly may affect alveolar macrophages (AMs) and epithelial cells (Øvrevik *et al.*, 2015). Various amounts of trace metals, polycyclic aromatic hydrocarbons (PAHs) and nitroarenes may adsorb to the surface of DEP. Characteristics of DEP are affected by fuel source, engine-type and operating conditions, and their chemical variability has implications for toxicological outcomes (Øvrevik *et al.*, 2015; Westerholm and Egebäck, 1994). Although the importance of DNA-damaging effects of DEP in lung carcinogenesis are well-accepted, the more precise role of oxidative stress and inflammatory reactions are not fully characterized (Cassee *et al.*, 2013; Øvrevik *et al.*, 2015). Many studies have addressed toxicity of DEP/DEP-extracts in different cell lines, but studies concerning effects of whole particles in normal human bronchial epithelial cells (HBECs) are less frequent (Schwarze *et al.*, 2013).

Airway epithelial cells have been shown to be important in mediating innate immune responses and inflammatory signaling (Bals and Hiemstra, 2004). Sustained inflammation and cellular redox imbalance may cause genomic instability leading to abnormal cells that are prone to malignant transformation. An important event in transforming epithelial cells to cancer cells is epithelial-to-mesenchymal transition (EMT), which is a reversible process also involved in tissue-repair and development of fibrosis (Kalluri and Weinberg, 2009; Lamouille *et al.*, 2014). Several genetic and epigenetic alterations may participate in the so-called cadherin-switch, with downregulation of E-cadherin and upregulation of N-cadherin in addition to upregulation of the mesenchymal cytoskeleton marker vimentin (Lamouille *et al.*, 2014; Liu *et al.*, 2015). The transcription factors SNAI1/2, ZEB1/2, and TWIST1 all participate in repression of E-cadherin, whereas TWIST1 may also be involved in induction of N-cadherin (Pallier *et al.*, 2012; Peinado *et al.*, 2007).

In vitro cell transformation due to DEP/DEP-constituents has been little studied in HBECs with a normal phenotype. Primary rat tracheal epithelial cells were transformed *in vitro* after exposure to SRM1650-extracts, but the cells did not gain immortalization (Ensell *et al.*, 1998). Another study showed that BALB/c-3T3 cells treated with DEP from a light-duty engine formed foci of morphologically transformed cells that were tumorigenic in nude mice (Hasegawa *et al.*, 1988). HBECs immortalized with *hTERT* and *CDK4* have been suggested to represent particularly relevant models for *in vitro* lung carcinogenesis (Delgado *et al.*, 2011; Ramirez *et al.*, 2004), compared with cell lines of either cancer origin or viral oncogene immortalization (ie, A549 and BEAS-2B) (Gazdar *et al.*, 2010). Two recent studies established stably transformed HBECs after long-term exposure to benzo[*a*]-pyrene (B[*a*]P) or cigarette smoke condensate (CSC) (Bersaas *et al.*, 2016; Vaz *et al.*, 2017). Transformation of HBECs following exposure to methylnitrosourea or B[*a*]P-diol-epoxide-1, either alone or in combination, has also been reported (Damiani *et al.*, 2008). B[*a*]P and chemical species in CSC are also present in various concentrations in DEP; however, the transformation potential of intact DEP in HBECs has, to our knowledge, not been investigated.

Enzymatic and nonenzymatic oxidation of arachidonic acid (AA) yields eicosanoids with implications for inflammation and carcinogenesis. Lipid mediators, including prostaglandins (PGs), are important signaling molecules with different and sometimes opposing functions, depending on tissue and body homeostasis, as well as environmental influences (Menter and Dubois, 2012). The implication of PGE_2 in inflammation and cancer is well documented (Menter and Dubois, 2012). $PGF_{2\alpha}$, the oxidation product of both PGE_2 and PGH_2, is also an important mediator of inflammatory responses. In contrast, isoprostanes like 8-iso-$PGF_{2\alpha}$ from nonenzymatic lipid peroxidation of AA, are markers of oxidative stress (Morrow *et al.*, 1990). Primary canine AMs exposed to 100 μg DEP/ml (SRM1650a) were shown to induce formation of AA, PGE_2, and 8-iso-$PGF_{2\alpha}$ (Beck-Speier *et al.*, 2005). In a study of primary rat AM exposed to low concentrations (1 and 10 μg/ml) of low sulfur DEP, release of PGE_2 was induced, whereas higher concentrations (100 and 500 μg/ml) attenuated the responses (Bhavaraju *et al.*, 2014). Consequently, altered secretion of eicosanoids could potentially serve as mediators of DEP-exposure. However, little is known about release of eicosanoids from HBECs after exposure to DEP.

Here, the potential of the chemically well characterized DEP reference material NIST SRM2975 to transform immortalized HBEC3 *in vitro* was studied. Several DEP-transformed clones were established and characterized for EMT-markers, and 1 clone (T2-HBEC3) was subjected to further studies. Baseline differences in gene expression profiles between parental HBEC3 and T2-HBEC3 were analyzed. Next, to assess differences in sensitivity to DEP, HBEC3 and T2-HBEC3 were characterized after short-term exposure by gene expression profiling, analysis of DNA strand breaks, as well as cellular release of Interleukin-1 beta (IL-1β) and eicosanoids.

MATERIALS AND METHODS

Sonication of the DEP material. Diesel particulate matter SRM2975 (collected from the exhaust of an industrial forklift) was purchased from NIST (National Institute of Standards and Technology, Gaithersburg, Maryland). Particles were weighed and resuspended in dH_2O to a concentration of 10 mg DEP/ml. This suspension was sonicated for 15 min at 4°C with amplitude 100% and cycle 0.5 (Hielscher Ultrasound Technology, Teltow, Germany) before aliqotation and freezing at −20°C. Before suspension in exposure media, DEP aliquots were thawed and sonicated 1 min at 4°C, peak power 75.0, duty factor 5.0 and cycles/burst 200 (Covaris M220 Focused-Ultrasonicator, Brighton, United Kingdom).

Nanoparticle tracking analysis. The mean hydrodynamic size of the suspended particles (DEP mode) was determined via

nanoparticle tracking analysis (NTA) using a NanoSight NS300 instrument (Malvern Instruments Ltd, Skallestad, Norway). DEP (100 μg/ml) was prepared and sonicated as indicated above and incubated in triplicates at 37°C. After 0, 24, and 72 h 2 μl aliquots were taken from each replicate and diluted in cell culture media (1:750). This dilution was used for NTA. Per measurement, 6 movies of 30 s each were recorded. All data were analyzed with the NanoSight NTA 3.1 software (Malvern Instruments Ltd, Skallestad, Norway). The results shown are from 3 independent measurements in triplicate.

Cell culture. The *hTERT* and *CDK4* immortalized normal HBEC line HBEC3 was kindly provided by Dr John D. Minna (Ramirez *et al.*, 2004). HBEC3 was recently authenticated by the Leibniz-Institut DSMZ (Deutsche Sammlung von Mikroorganismen und Zellkulturen GmbH, Braunschweig, Germany). HBEC3 were maintained in a mixture (1:1) of LHC-9 (Thermo Fisher Scientific, Oslo, Norway) and RPMI 1640 (Sigma-Aldrich, Oslo, Norway) medium with 5% fetal bovine serum (Sigma-Aldrich), and plated on collagen coated (Nutragen, CellSystems, Troisdorf, Germany) dishes (Sarstedt, Oslo, Norway). Cells were maintained at 37°C in humidified atmosphere with 5% CO_2.

High-resolution field emission scanning electron microscopy. HBEC3 cells were seeded at 2600 cells/cm^2 onto collagen coated 24 mm Costar Transwell Permeable Support 0.4 μm Polycarbonate Membrane (Thermo Fisher Scientific) and placed in the incubator for 24 h. Two wells without cells were included as controls. Cells were exposed to 0 and 100 μg DEP/ml for 72 h whereas wells without cells were exposed to 100 μg DEP/ml only. After 72 h, the exposure media were discarded and the wells were washed twice with PBS before fixation in 10% neutral buffered formalin-PBS-solution (Sigma-Aldrich). Samples were then dehydrated using gradients of ethanol (EtOH) (Kemethyl, Kolbotn, Norway followed by a chemical drying series with Hexamethyldisilazane (Sigma-Aldrich) and EtOH.

The filter specimens were cut from the exposure wells and mounted on a 25-mm diameter aluminum pin stub (Agar Scientific Ltd., Stansted Essex, United Kingdom). Samples were air-dried under sterile conditions for approximately 1 h at RT before being mounted on specimen mounting stubs of 25 mm (Agar Scientific Ltd.). Double-sided carbon adhesive discs (Agar Scientific Ltd.) were used for mounting the specimens onto the stubs. The stubs were then sputter coated with 5- to 6-nm thick layer of platinum in a Cressington 208HR sputter coater (Cressington Scientific Instruments Ltd., Watford, United Kingdom). Samples were analyzed using a SU 6600 Field emission scanning electron microscopy (FESEM) (Hitachi, Ibaraki-ken, Japan) in the secondary electron imaging mode. The microscope was operated at an acceleration voltage of 10.0 kV, an extraction voltage of 1.8 kV, and a working distance of 7.4 and 7.7 mm.

DEP cell transformation assay. HBEC3 were seeded at 1.0×10^4 cells/well in quadruplicates in 6-well plates (Nunc, Thermo Fisher Scientific) and exposed to the nontoxic concentration of 100 μg DEP/ml (15.6 μg/cm^2) for 72 h followed by 72 h with media only. Control cells were exposed to the same cell culture medium without DEP. Media were changed after 72 h. The 4 technical replicates for both control and exposed cells were treated independently throughout the assay. DEP-exposed and control cells were trypsinized, reseeded at 10 000 cells/well and treated as mentioned above for the next 15 weeks. After 15 weeks, cells were seeded in 0.35% soft agar (Difco agar noble, Sigma-Aldrich). After approximately 2 weeks, colonies ≥ 20 μm in diameter were counted. Colonies were isolated using a micropipette and transferred to a 24-well plate where monolayers of cells were established. The soft agar assay was carried out twice to ensure true clonality and continued potential of the isolated cell lines to grow anchorage-independently. Several cell lines were established. Based on the expression of EMT-marker genes, one of the cell lines, T2-HBEC3, was selected as a model for further studies.

Cell migration and invasion analysis. Cell migration and invasion was studied using an IncuCyte Zoom Live Cell Imaging microscope and software (Essen BioScience, Mölndal, Sweden). Cells were seeded at a concentration of 6.0×10^4 cells/well in an ImageLock 96-well plate coated with matrigel (100 μg/ml, Corning Matrigel, VWR International, Oslo, Norway). A wound was made in the cell layer by the WoundMaker tool (Essen BioSciences) after 16 h. To study migration, cells were placed in the incubator containing the IncuCyte Zoom microscope and images were acquired every hour for 72 h. To study invasion capacity, the cell layer was embedded in 8 mg/ml matrigel before the plate was placed in the incubator.

Immunoblotting analysis. Whole cell extracts of HBEC3 and T2-HBEC3 were prepared and protein concentrations were measured using the BCA Assay (Thermo Fisher). Protein samples (25 μg) were run on 10% Mini-Protean TGX Stain-Free gel (BioRad, Oslo, Norway) and transferred to a PVDF membrane (BioRad). Antibodies against vimentin (V6630, Sigma-Aldrich), β-actin (MA5-11869, Thermo Fisher Scientific) and E-cadherin (EP700Y, Abcam, Cambride, United Kingdom) were used. Secondary antibodies were horseradish peroxidase-conjugated antirabbit/antimouse IgG antibodies (Cell Signaling Technology, Leiden, The Netherlands). Immunoreactive bands were detected using chemiluminescent substrate (SuperSignal West Pico, Thermo Fisher Scientific).

Short-term exposure to DEP. To assess possible differences in responses to DEP-exposure in HBEC3 and T2-HBEC3, 2 short-term exposure experiments were conducted: (1) a dose-response experiment with exposure concentrations ranging from 0 to 400 μg DEP/ml for 48 h and 2) a time-course experiment where cells were exposed to 200 μg DEP/ml for 24, 48 and 72 h, respectively. Following these exposures, several endpoints were analyzed, including gene expression profiling, analysis of DNA strand breaks, and cellular release of IL-1β and eicosanoids.

HBEC3 and T2-HBEC3 were seeded in triplicates into collagen coated 6-well plates (Nunc) at 2.0×10^5 cells/ml and left in the incubator for 24 h. Cells were then exposed either to different concentrations of DEP (0, 25, 50, 100, 200, and 400 μg/ml) (corresponding to 3.9, 7.8, 15.6, 31.3, and 62.5 μg/cm^2) for 48 h ("dose-response") or to 200 μg DEP/ml (31.3 μg/cm^2) for 24, 48, and 72 h ("time-course"). Exposure media were collected at the end of the exposures, centrifuged at 4°C, 12 000 rpm for 10 min to discard particles and stored at −20°C until further analyses. Cells on the 6-well plates were washed ×3 in ice-cold PBS and stored at −80°C for isolation of RNA.

Measurement of gene expression by RT-qPCR. Total RNA was isolated from exposed cells with Isol-RNA Lysis Reagent (5 Prime, VWR International, Oslo, Norway) and dissolved in nuclease free water. RNA quantity and quality were measured with Nanodrop 8000 (Thermo Fisher Scientific) and integrity of the

isolated RNA was ascertained on an Agilent Bioanalyzer by the use of RNA 6000 Nano kit (Agilent Technologies, Oslo, Norway). RIN values were in all cases ≥ 9. One μg of total RNA was used as input for reverse transcription with qScript cDNA synthesis kit (Quanta Biosciences, VWR International, Oslo, Norway). qPCR reactions were set up with PerfeCTa SYBR green fast mix (lo/high ROX) (Quanta Biosciences, VWR International) and run on StepOnePlus (Applied Biosystems, Thermo Fisher Scientific) or Quant Studio 5 (Applied Biosystems, Thermo Fisher Scientific). Relative gene expression was normalized to the expression of *β-actin* and calculated using the ΔΔCt method. Primers were purchased from Sigma-Aldrich or Thermo Fisher Scientific. Primer sequences used in this study are summarized in the Supplementary Table 1.

Gene expression profiling. Biotinylated complementary RNA (cRNA) was generated from 500 ng of total RNA (RIN ≥ 9) using the TargetAmp-Nano Labeling Kit for Illumina Expression BeadChip (Epicentre, an Illumina company, Madison, WI). Biotinylated cRNA targets (900 ng) was hybridized to the Illumina Human-HT12 v4 Expression BeadChips for 17 h at 58°C. Hybridization, as well as the subsequent washing, staining, and drying of the beadchips were performed according to the standard Illumina protocol. The hybridized beadchips were scanned using the Illumina iScan System and bead level data were summarized by Illumina GenomeStudio Software v2011.1 (Illumina Inc., GeneTiCA, Prague, Czech Republic). Normalized and raw bead level data are deposited in GEO with accession number GSE107481.

Measurement of cytokine release by ELISA. IL-1β release to cell culture media from the DEP dose-response experiments was measured by ELISA using the Human IL-1β/IL-1F DuoSet kit (R&D system Europe, Abingdon, United Kingdom) according to the manufacturer's instructions. Absorbance was measured and quantified using a TECAN sunrise plate reader with associated software (Magellan V 1.10, Phoenix Research Product, Hayward, California).

Comet assay. Cells were exposed to different concentrations of DEP (0, 25, 50 and 100 μg/ml) for 24 h. Cells were trypsinized and resuspended (1×10^6 cells/ml) in PBS (10 mM EDTA, without Ca^{2+}/Mg^{2+}, pH 7.5) before resuspension in 0.75% soft agar solution. In total 7 μl of this suspension was loaded in triplicates onto hydrophilic polyester films (GelBond, Lonza Rockland Inc., Maine) and lysed over night at 4°C. For analysis of oxidative DNA-damage, films were first treated for 1 h at 4°C in enzyme buffer (40 mM HEPES with 0.1 M KCl and 0.5 mM Na_2-EDTA, pH 7.6) and then for 1 h at 37°C with/without 0.5 μg/ml formamidopyrimidine-DNA-glycosylase (FPG) in enzyme buffer containing 0.2 mg/ml BSA. The FPG enzyme (crude FPG extract) was prepared with modifications as described in Olsen *et al.* (2003). DNA was unwinded by immersing the films in cold electrophoresis solution (0.3 M NaOH, 0.001 M Na_2-EDTA, pH > 13) for 40 min and electrophoresis was run at 10°C with 0.8 V/cm for 25 min with circulation as described previously in Gutzkow *et al.* (2013). After fixation in 96% EtOH, DNA was stained with SYBR GoldNucleic Acid Gel Stain (Life Technologies, Paisley, United Kingdom) diluted 1:10 000 in TE-buffer (1 mM Na_2-EDTA, 10 mM Tris-HCl, pH 8) before examination at ×20 magnification under Olympus BX51 microscope (light source: Olympus BH2-RFL-T3, Olympus Optical Co., Ltd.; camera: A312f-VIS, BASLER, Ahrensburg, Germany). Approximately 30 comets per gel were randomly counted (Comet Assay IV, Perceptive Instruments, Suffolk, United Kingdom) and DNA-damage was quantified as tail intensity (% tail DNA).

Liquid-chromatography-tandem-mass-spectrometry analysis of eicosanoids. Standards of PGE_2, PGD_2, PGA_2, PGI_2, PGJ_2, $PGF_{2\alpha}$, 8-iso-$PGF_{2\alpha}$, 8-iso-PGE_2, 15-keto-PGE_2, 13, 14-dihydro-15-keto-PGE_2, 13, 14-dihydro-15-keto-PGD_2, and lipoxin A4 (LXA4) were purchased from Cayman Chemical Company (Michigan). Hydroxyeicosatetraenoic acids (HETEs), epoxyeicosatrienoic acid, formic acid puriss p.a. for mass spectroscopy, ethyl acetate p.a. ACS, methanol p.a. ACS and acetonitrile liquid-chromatography-tandem-mass-spectrometry (LC-MS) grade were purchased from Sigma-Aldrich (Prague, Czech Republic). Ultrapure water was obtained from a Milli-Q UF Plus water system (Millipore, Molsheim, France).

Solid-phase-extraction was used for extraction of AA metabolites from cell culture media. SELECT HLB SPE 1 ml (30 mg) cartridges (Supelco, Prague, Czech Republic) were washed with 1 ml of ethyl acetate, 1 ml of methanol and 1 ml of water. Then 1 ml of cell culture medium was loaded onto each SPE column. The columns were washed with 2 ml of water. The cartridges were air dried for 3 min with vacuum and analytes were eluted with 1.5 ml of methanol. Samples were dried under a stream of nitrogen, re-dissolved in 60 μl of methanol and aliquots of 5 μl were injected into the HPLC column.

Sample analyses were performed using LC/MS/MS. An Agilent 1200 chromatographic system (Agilent Technologies, Waldbronn, Germany), consisting of binary pump, vacuum degasser, auto sampler and thermostatted column compartment, was used. Separation of PGs was carried out using an Ascentis Express C18, 2.1 × 150 mm, 2.7 μm particle size column (Supelco, Bellefonte, Pennsylvania) with a 25-min linear gradient from 30% to 100% of acetonitrile. Mobile phase contained 0.1% of formic acid. The flow rate of the mobile phase was 0.3 ml/min, the column temperature was set at 45°C. A triple quadrupole mass spectrometer Agilent 6410 Triple Quad LC/MS (Agilent Technologies, Santa Clara) with an electrospray interface (ESI) was used for detection of the analytes. The mass spectrometer was operated in the negative ion mode. Selected ion monitoring at m/z 303.2 was used for quantification of AA and multiple reaction monitoring for other analytes.

Statistical analysis. Data output was analyzed in Sigma Plot 12.0, RStudio (2009) or StataSE 14. Mann-Whitney *U* test was used when analyzing soft agar colony formation. Multiple comparisons of DEP-transformed clones were conducted with ANOVA on log-transformed data with Dunnett's post hoc test. The dose-response experiments were analyzed by a linear mixed model (nlme package in R), with a random intercept for combinations of experiment, dose, and cell line. The residual variance was allowed to vary between cell lines. Data from time-course exposure experiments were analyzed by a linear mixed model (Stata), with random intercept for experiment. Data from migration patterns were analyzed by a non-linear mixed effects model using the nlme package (R). We considered here the following model $D[1 - \exp(-B \times \text{hour} - C \times \text{hour}^2)]$ where B indicates the cells migration rate, and D indicates the final asymptotic cell density in the wound. The C coefficient, a constant value, was added to give a closer fit between model predictions and data. Both B and D had cell line as fixed effect. In addition, nested random intercepts for cell line, experiment and well were added for B, allowing the migration rate to vary between cell lines, experiments and wells.

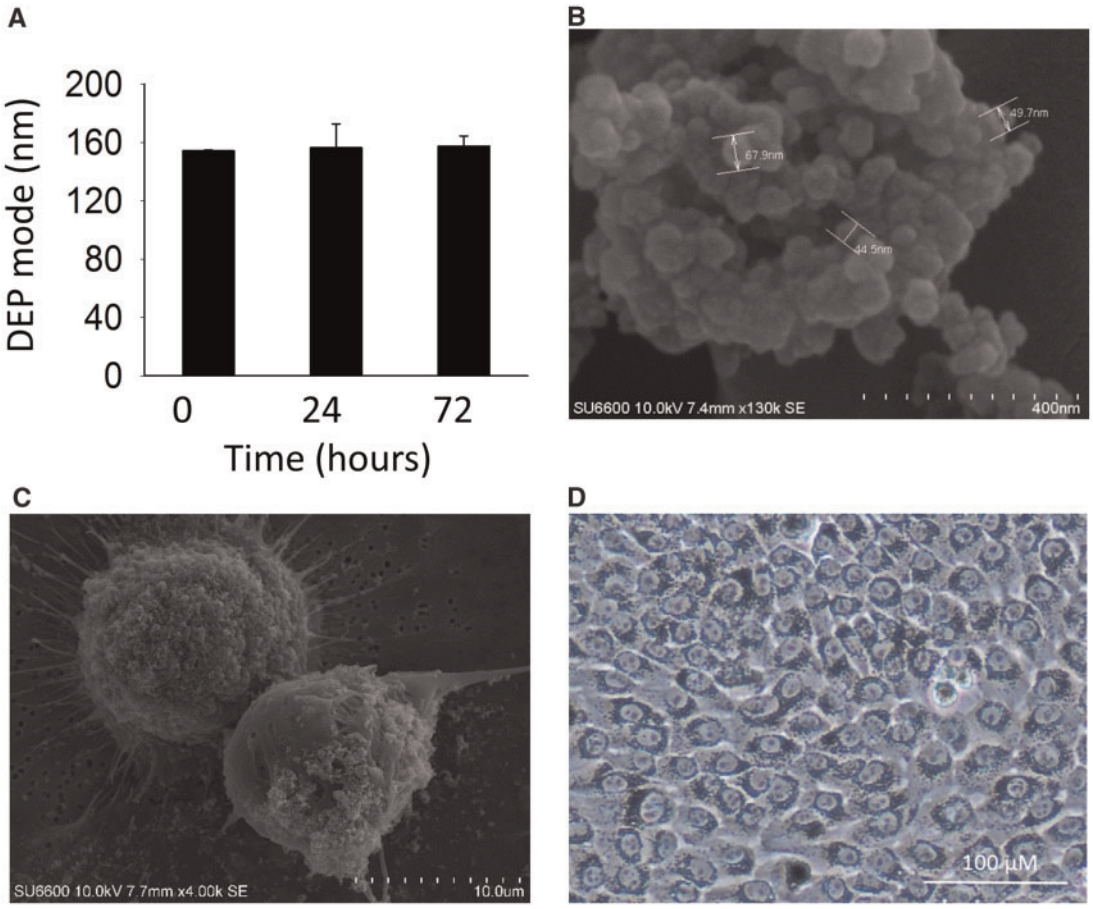

Figure 1. Exposure of cells to DEP. A, Mean hydrodynamic size of SRM2975 (DEP) in cell culture medium incubated for 0–72 h after ultrasonication. Data display mean ± SD, $n = 3$. FESEM images of DEP dispersed in cell culture medium (B) and HBEC3 exposed to 100 μg DEP/ml for 72 h (C). D, Light microscopy image (×10 magnification) of HBEC3 exposed to 100 μg DEP/ml for 48 h.

Bead summary data from microarray analysis were imported into the R statistical environment (http://www.r-project.org; last accessed April 2017) and normalized using the quantile method in the Lumi package (Du *et al.*, 2008). Only probes with a detection p-value $< .01$ in >50% of arrays were included for further analyses. Differential gene expression was analyzed in the Limma package using the moderated t-statistic. A linear model was fitted for each gene given a series of arrays using lmFit function. Multiple testing correction was performed using the Benjamini and Hochberg method. ToppFun tool was utilized for annotated genes. Goeman's global test and the KEGG database (http://www.genome.jp/kegg; last accessed April 2017) were applied to identify deregulated biological pathways and deregulated genes within these pathways. The procedure of Holm for control of the family wise error rate was applied.

RESULTS

Exposure of HBEC3 to SRM2975

The mean hydrodynamic size of ultrasonicated DEP dispersed in cell culture medium was approximately 150 nm in diameter and did not change with time (0–72 h) (Figure 1A). FESEM images were acquired for DEP dispersed in cell culture medium showing core particles with a diameter of approximately 50 nm (Figure 1B), and HBEC3 cells exposed to 100 μg DEP/ml for 72 h showed DEP attached to the cell surface (Figure 1C). Further examination by light microscopy of HBEC3 exposed to 100 μg DEP/ml for 48 h after washing indicated black staining from the particles also colocalizing with cell cytoplasm. There was a lack of staining above nuclei and at the outer edge of the cell membranes, suggesting intracellularly localization of DEP (Figure 1D).

HBEC3 In Vitro Transformation Assay

HBEC3 was exposed to the subtoxic concentration of 100 μg DEP/ml for 15 weeks before seeding in soft agar. After 14 days in soft agar, a significant increase in colony growth from DEP-exposed cells compared with controls was observed (Figure 2A). The transformation efficacy (TE) was 0.39%. Single colonies were picked from the soft agar and transferred to monolayer culture. To ensure continued potential to grow anchorage-independently in soft agar and to verify clonal origin, transformed cells were subjected to a second round of selection in soft agar. Four DEP-transformed clones were subsequently established as cell lines in monolayer culture and subjected to further investigation of expression of EMT-marker genes.

DEP-Transformed Clones Express Markers of EMT

Expression of several genes known to be involved in EMT was analyzed in 4 DEP-transformed clones. All clones showed significantly reduced expression of *CDH1* compared with the parental cell line HBEC3, while the levels varied between the individual clones (Figure 2B). Three of the clones showed upregulation of *CDH2* expression, whereas the level of expression from clone

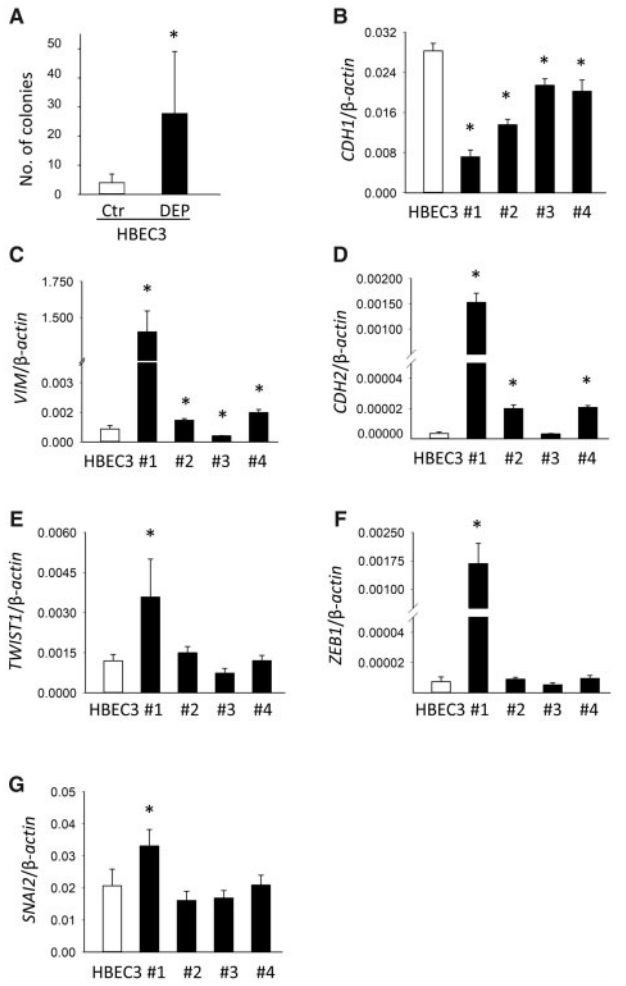

Figure 2. DEP-induced *in vitro* transformation and expression of EMT-marker genes. A, Colony formation in HBEC3 exposed to 100 μg DEP/mL for 15 weeks compared with unexposed control cells. Data display mean ± SD, $n = 4$. * $p < .05$ (Mann-Whitney *U* test). EMT-marker genes were measured in HBEC3 and DEP-transformed clones Nos. 1–4: (B) *CDH1*, (C) *VIM*, (D) *CDH2*, (E) *TWIST*, (F) *ZEB1*, and (G) *SNAI2*. Gene expression levels were measured by qRT-PCR and normalized to *β-actin* ($2^{-\Delta\Delta Cq}$) (mean ± SD, $n = 3$). *$p < .05$ (ANOVA).

No. 3 was similar as to HBEC3 (Figure 2C). Significantly altered expression of *VIM* was measured in all clones compared with HBEC3. Whereas the expression of *VIM* was significantly higher in clone Nos. 1, 2, and 4, it was significantly lower in clone No. 3 compared with HBEC3 (Figure 2D). Only clone No. 1 showed significantly different expression of *TWIST1*, *ZEB1*, and *SNAI2* compared with HBEC3 (Figs. 2E–G). Clone No. 1 (as from here on termed T2-HBEC3) showed the clearest indications of EMT based on the expression of these EMT-marker genes, and was selected for further studies of DEP-induced transformation and toxicity. HBEC3 possess an epithelial morphology (Figure 3A), and T2-HBEC3 have a larger, more spindle-shaped mesenchymal/fibroblasts-like morphology (Figure 3B). Downregulation of E-cadherin and induction of vimentin proteins in T2-HBEC3 was also evident by immunoblotting (Figure 3C).

Migratory and Invasive Potential of HBEC3 and T2-HBEC3

A scratch wound closure assay was performed with HBEC3 and T2-HBEC3. Interestingly, T2-HBEC3 displayed a significantly slower migration pattern compared with HBEC3 (Figure 3D). HBEC3 completely closed the wound after 6 h, whereas T2-HBEC3 closed the wound after 48 h. Neither HBEC3 (data not shown) nor T2-HBEC3 (Figure 3E) had the capability to invade a reconstituted matrigel during the 48 h observation period.

Gene Expression Profiling

First, gene expression profiling was carried out on baseline samples of HBEC3 and T2-HBEC3 to explore intrinsic differences between the 2 cell lines. 429 genes (224[↑] and 205[↓]) were found to be significantly deregulated between HBEC3 and T2-HBEC3 and the 48 most significantly up- and down-regulated genes at baseline are presented in Table 1. Utilizing the ToppFun-tool, several of these genes were identified as being involved in i.e. regulation of cell migration and lung carcinogenesis: (*DNER*[↑], *FBLN1*[↑], *HBEGF*[↓], *IGFBP3*[↑], *LAMA4*[↑], *PROS1*[↑], *RAB25*[↓], *SPOCK1*[↑], *ST14*[↓], *TGFBR3*[↑], *TP53INP1*[↑], *CD9*[↓], *CLDN1*[↓], *DUSP6*[↓], *EPCAM*[↓], *EPHA1*[↓], *FOXA2*[↓], *HAS3*[↓], *HTRA1*[↑], *MUC1*[↑], *PMEPA1*[↑], *TIMP2*[↑], *EGR1*[↓], *EPHA1*[↓], *IL1B*[↓], and *VIM*[↑]).

At baseline there were 8 significantly deregulated pathways (KEGG database) between HBEC3 and T2-HBEC3 having particular implications for *in vitro* carcinogenesis: "*Axon guidance*", "*Focal adhesion*" and the "Mitogen-activated protein kinase (MAPK)-", "*Insulin-*", "*Toll-like receptor-*", "*TGF-β-*", "*Hedgehog-*", and "The mechanistic target of rapamycin (mTOR)-" signaling. A complete list of significantly deregulated pathways at baseline is presented in Supplementary Table 2A.

Next, to assess differences in toxic effects of DEP between the parental HBEC3 and T2-HBEC3, gene expression profiling was carried out on selected samples from DEP short-term exposure experiments. This included exposure to 50 or 200 μg DEP/ml for 48 h, and 200 μg DEP/ml for 24 or 72 h. In the dose-response experiments, more genes were deregulated after exposure to the highest concentration (200 μg DEP/ml) compared with 50 μg DEP/ml for both cell lines (Figure 4A). 16 genes were deregulated at both DEP-concentrations in HBEC3, while in T2-HBEC3 there were 15 common deregulated genes (Figure 4B). It is interesting to note that the only gene that was altered by the 2 DEP-exposures in both cell lines is *CYP1B1*. In the time-course experiment, more genes were deregulated after 72 h than after 24 h of exposure (200 μg DEP/ml) for both cell lines (Figure 4C). In total 3 genes were deregulated at both exposure times in HBEC3, while in T2-HBEC3 there were 4 common deregulated genes (Figure 4D).

A comprehensive overview of significantly affected pathways from DEP short-term exposure experiments is presented in Supplementary Tables 2B–I. Pathways significantly deregulated at 2 or more exposure scenarios (ie, in either experiment) are presented in Table 2. A full list of deregulated genes associated with each pathway at the different exposure scenarios is presented in Supplementary Table 3.

Four pathways were commonly deregulated in both HBEC3 and T2-HBEC3 in the short-term DEP-exposure experiments: "*Tryptophan metabolism*", "*Valine, leucine and isoleucine degradation*", "*Terpenoid backbone biosynthesis*" and "*Steroid biosynthesis*". Three pathways were significantly deregulated in HBEC3, only: "*Metabolism of xenobiotics by cytochrome p450*", "*Phagosome*", and "*Aldosterone-regulated sodium reabsorption*". In T2-HBEC3, several pathways associated with inflammatory responses were identified in addition to "*Synthesis and degradation of ketone bodies*", "*Butanoate metabolism*", and "*Pyruvate metabolism*".

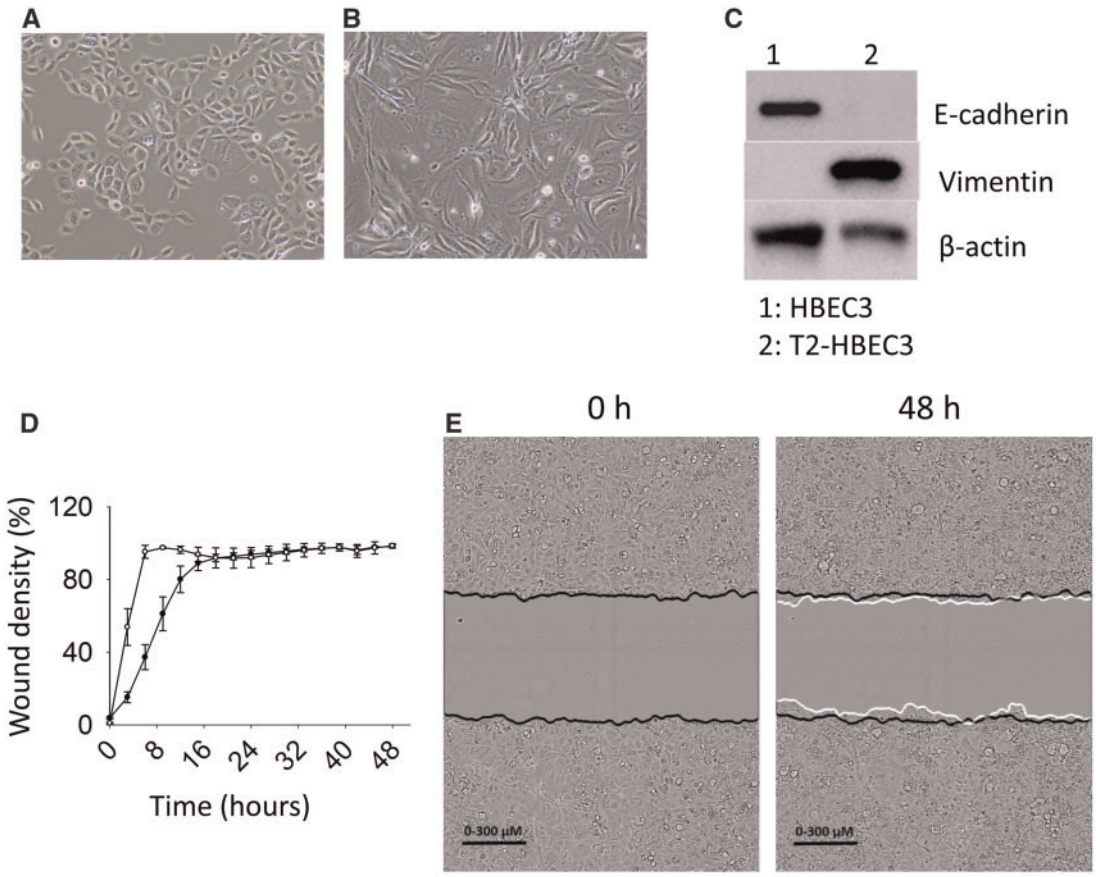

Figure 3. Morphology, and migratory and invasive potential. Light microscopy images (×10 magnification) of HBEC3 (A) and T2-HBEC3 (B). C, E-cadherin and vimentin protein levels were analyzed in HBEC3 and T2-HBEC3 by immunoblotting. β-actin was used as loading control. Migration and invasion were measured in a scratch wound closure assay. D, HBEC3 (○) and T2-HBEC3 (•) display significantly different migration curves. Data display wound density (percent) ± SE, $n = 3$. $p < 0.05$ (non-linear mixed effects model). E, Invasive potential of T2-HBEC3 analyzed by live cell imaging. Black lines display the original scratch wound made in the cell layer at 0 h and the white lines display the invading front of cells after 48 h.

Expression of CYP1A1, CYP1B1, and IL1B

Selected genes involved in xenobiotic metabolism and inflammation were measured by RT-qPCR in HBEC3 and T2-HBEC3 from the DEP short-term exposure experiments. In the dose-response experiment, gene expression of *CYP1A1* increased significantly for both cell lines starting at the lowest concentration of 25 μg DEP/ml (Figure 5A). For concentrations ranging between 50 and 400 μg DEP/ml, significantly higher induction of *CYP1A1* was observed for T2-HBEC3 compared with HBEC3. Expression of *CYP1A1* increased significantly with time for both cell lines (Figure 5B), but for HBEC3 induction was only statistically significant after 48 and 72 h. Induction of *CYP1B1* was also found in the short-term exposure experiments (Supplementary Figure 1A).

By gene expression profiling, *IL1B* was among the genes showing the most differential expression between HBEC3 and T2-HBEC3 at baseline (Table 1). When measured by RT-qPCR, HBEC3 showed generally higher expression of *IL1B* than T2-HBEC3 (Figure 5C). Expression of *IL1B* increased dose-dependently for both cell lines at the 3 highest exposure concentrations (100–400 μg DEP/ml). In the time-course experiment, significantly increased expression of the *IL1B* gene was found for both cell lines at all time-points (200 μg DEP/ml), but no differences between the cell lines were observed (Figure 5D). Higher levels of IL-1β protein were identified at all concentrations (0–400 μg DEP/ml) in culture media from HBEC3 compared with T2-HBEC3 (Figure 5E). Induction of *IL1A* was also found in the short-term DEP-exposure experiments (Supplementary Figure 1B). In addition, the *IL-6*, *IL-8* and *TNF-α* genes were measured, but their levels of expression were at or below the detection limit.

Analysis of DNA Strand Breaks

DNA strand breaks/alkali-labile sites were measured in HBEC3 and T2-HBEC3 exposed to 0, 25, 50, and 100 μg DEP/ml for 24 h. Significantly increased levels in DNA strand breaks were observed for both cell lines at all DEP concentrations, but there were no indications of dose-response relationships (Figure 5F). Increased oxidative DNA-damage associated with FPG sensitive sites was not observed (data not shown).

Effects of DEP-Exposure on Cellular Secretion of Eicosanoids

The effect of DEP-exposure on release of AA and several AA metabolites (Supplementary Table 4) into cell culture media was measured. Although the levels of lipoxygenase metabolites (5-, 8-, 12-, and 15-HETE) and LXA4 secreted into the growth medium were not changed (data not shown), AA and PG production was significantly affected by exposure to DEP. Secretion of AA was significantly higher in T2-HBEC3 than in HBEC3 at all concentrations (0–400 μg DEP/ml) in the dose-response experiments (Figure 6A). With HBEC3, but not T2-HBEC3, there was a reduction of secreted AA at the exposure concentrations 25–400 μg

Table 1. The 48 Most Significantly Deregulated Genes Between HBEC3 and T2-HBEC3 at Baseline

Symbol	log2FC	Symbol	log2FC
VIM	6.33	LAD1	–2.04
CPA4	4.26	CD9	–2.05
FBLN1	4.05	REPIN1	–2.06
SRGN	3.78	KRT18P13	–2.08
IGFBP3	3.77	DUSP6	–2.12
LOX	3.50	ST14	–2.13
CA9	3.45	EPHA1	–2.14
GAS1	3.44	CLDN1	–2.18
SVEP1	3.00	HBEGF	–2.21
SAMSN1	2.94	FOXA2	–2.22
CYBRD1	2.94	EGR1	–2.24
DKK1	2.89	TMEM30B	–2.25
SPOCK1	2.87	RAB25	–2.40
MXD4	2.85	UPP1	–2.41
MME	2.81	FGFBP1	–2.62
PROS1	2.64	HAS3	–3.14
HTRA1	2.49	IL1B	–3.82
SEZ6L2	2.48	EPCAM	–4.55
DHRS9	2.32		
DNER	2.31		
MUC1	2.31		
LAMA4	2.31		
PMEPA1	2.18		
TP53INP1	2.17		
TIMP2	2.14		
COL8A1	2.14		
TGFBR3	2.11		
NNMT	2.09		
MFGE8	2.09		
RPS6KA2	2.08		

The table display the 48 most significantly deregulated genes between baseline HBEC3 and T2-HBEC3 identified from gene expression profiling.
$p < 0.001$ and log2FC < -2.0 and > 2.0 (moderated t-statistics).

DEP/ml, compared with control. In the time-course experiment, exposure to 200 μg DEP/ml resulted in a reduction in AA secretion at all time-points from HBEC3 and after 48 and 72 h from T2-HBEC3, compared with the respective controls (Figure 6A).

PGs PGE_2 and $PGF_{2\alpha}$ were the major AA metabolites identified. Secretion of PGE_2 and $PGF_{2\alpha}$ (Figs. 6B and 6C) increased dose-dependently for HBEC3 only, in the range of exposure concentrations from 100 to 400 μg DEP/ml. Generally, higher levels of PGE_2 and $PGF_{2\alpha}$ secretion were found from T2-HBEC3 compared with HBEC3. PGE_2 secretion increased significantly after DEP-exposure in HBEC3 at all time-points (200 μg DEP/ml) compared with the respective controls. At 72 h of exposure, a higher increase in PGE_2 secretion was found in HBEC3 (4-fold) compared with T2-HBEC3 (<2-fold). Whenc compared with controls, there was increased secretion of $PGF_{2\alpha}$ from DEP-exposed (200 μg/ml) HBEC3 at all time-points. At 24 h, an increase (2-fold) of $PGF_{2\alpha}$ secretion was found in HBEC3 whereas with T2-HBEC3 a minor reduction was observed.

In accordance with the observed increase in PGE_2, PGA_2, which is a product of subsequent nonenzymatic 15-oxidation and 13, 14-reduction of PGE_2, was also measured. Unchanged levels of PGA_2 were found from T2-HBEC3 only, in the dose-response experiment. In the time-course experiment, significantly increased PGA_2 levels were identified in both cell lines. However, 1 or 2 orders lower concentrations of PGA_2 were found, compared with PGE_2 and $PGF_{2\alpha}$ (Supplementary Figure 3A). Secretion of 13, 14-DH-15-keto-PGE_2, the downstream product of $PGF_{2\alpha}$, decreased significantly for T2-HBEC3 at the highest exposure (400 μg DEP/ml), meanwhile it did not change for HBEC3 at any concentration (Figure 6D). 13, 14-DH-15-keto-PGE_2 secretion levels were reduced with time after 200 μg DEP/ml for HBEC3 after 48 and 72 h compared with the respective controls.

Levels of PGI_2 and PGD_2, ie, products of 2 other AA metabolic pathways, were not modulated by DEP (data not shown); however, a significant increase in release of PGJ_2 (a direct downstream metabolite of PGD_2) was found in HBEC3 at 50–400 μg DEP/ml, compared with control (Supplementary Figure 3B), suggesting that also the alternative PG synthase pathway is induced in HBEC3. Interestingly, no PGJ_2 was identified in T2-HBEC3.

Importantly, the levels of 8-iso-$PGF_{2\alpha}$, a biomarker of membrane lipid peroxidation, increased significantly for HBEC3 at the 3 highest exposure concentrations (100–400 μg DEP/ml) (Figure 6E). Higher levels of 8-iso-$PGF_{2\alpha}$ were found in T2-HBEC3 compared with HBEC3 at 0, 25, and 400 μg DEP/ml. Secreted levels of 8-iso-$PGF_{2\alpha}$ increased with time for T2-HBEC3 only.

Identification of Deregulated Genes Involved in AA Metabolism

Based on the results from eicosanoid secretion, gene expression profiling data was explored to look for genes that could aid in explaining the observed changes in AA metabolism. In T2-HBEC3 compared with HBEC3 exposed to 200 μg DEP/ml for 24 h, deregulation of *PLA2G2A*(↑), *PLA2G10*(↑), *ALOX5*(↑), *CYP2J2*(↑), *LTA4H*(↑), *AKR1C3*(↑) was found (Supplementary Table 2H). This pathway was also deregulated in T2-HBEC3 compared with HBEC3 after 48 h at all exposure concentrations (50–200 μg DEP/mL) (Supplementary Table 2F and G). In T2-HBEC3 compared with HBEC3 at 50 μg DEP/ml *ALOX5*(↑), *CYP2J2*(↑), *PTGES*(↑), *PLA2G2A*(↑), *COX-2*(↑), *CBR3*(↓), *GPX3*(↓), and *CYP4F11*(↓) were deregulated, meanwhile at 200 μg DEP/ml *ALOX5*(↑), *CYP2J2*(↑), *PLA2G2A*(↑), *COX-2*(↑), *GPX3*(↓), and *GPX2*(↓) were found to be altered. Verification of selected DEGs by RT-qPCR is found in Supplementary Figure 2.

DISCUSSION

This study reports that DEP (NIST SRM2975) transformed HBEC3 *in vitro*. Transformed clones showed varying degree of expression of EMT-markers. One clone, T2-HBEC3, gave marked indications of EMT and showed differences in baseline gene expression profiles when compared with parental HBEC3. T2-HBEC3 also showed altered sensitivity to short-term DEP-exposure regarding gene expression profiles and inflammatory markers.

Long-term DEP-exposed HBEC3 formed a significantly increased number of anchorage-independent colonies compared with unexposed cells. The present DEP *in vitro* transformation study is of particular importance as HBEC3 are genomically stable with intact tumor suppressor TP53 checkpoint, and show a low rate of spontaneous transformation (Damiani *et al.*, 2008; Ramirez *et al.*, 2004). The TE of 0.39% was low. A previous study with HBEC1 and HBEC2 exposed to methylnitrosourea and B[*a*]P-diol-epoxide-1 reported a TE of 0.2%–3.0% (Damiani *et al.*, 2008). B[*a*]P and several chemical species in CSC are present in various concentrations in DEP. However, this is the first time, to our knowledge, an immortalized HBEC line with a normal phenotype has been stably transformed following *in vitro* exposure to intact DEP with low content of organic compounds. The carcinogenic potential of DEP is debated (HEI Diesel Epidemiology Panel, 2015), highlighting the need for further studies

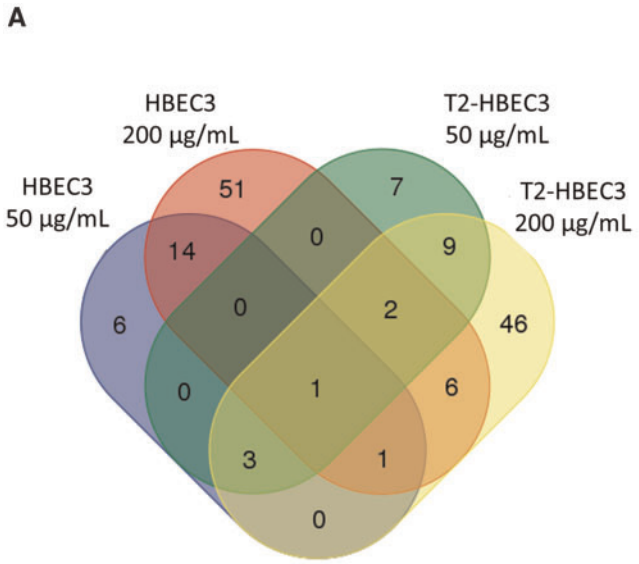

B

	HBEC3			T2-HBEC3	
	50 µg/mL	200 µg/mL		50 µg/mL	200 µg/mL
Genes	log2FC	log2FC	Genes	log2FC	log2FC
CYP1A1	2.67	2.23	INSIG1	1.71	2.47
CYP1B1	2.55	2.64	CYP1B1	2.30	2.78
RNY4	1.66	1.28	SC4MOL	1.85	2.33
EREG	1.47	0.75	SCD	1.44	1.72
ACSS2	1.24	1.49	LDLR	1.28	1.78
LIPG	1.10	0.73	SQLE	1.20	1.70
ITGB5	0.94	1.63	IER3	1.10	2.17
F3	0.90	1.76	FTH1	1.00	0.93
STC1	0.87	0.85	FDFT1	0.85	1.50
HMGCR	0.71	1.02	MTE	0.85	1.47
ABCC3	0.66	1.40	DKK3	0.64	1.06
ADRB2	-0.76	-1.32	EFEMP1	-0.75	-0.94
GLUL	-0.78	-1.47	ALDH1A1	-0.76	-1.05
DNAJC15	-1.00	-1.32	SEPP1	-0.96	-1.53
EPSTI1	-1.38	-1.60	C10orf99	-1.08	-1.99
CD24	-1.44	-2.10			

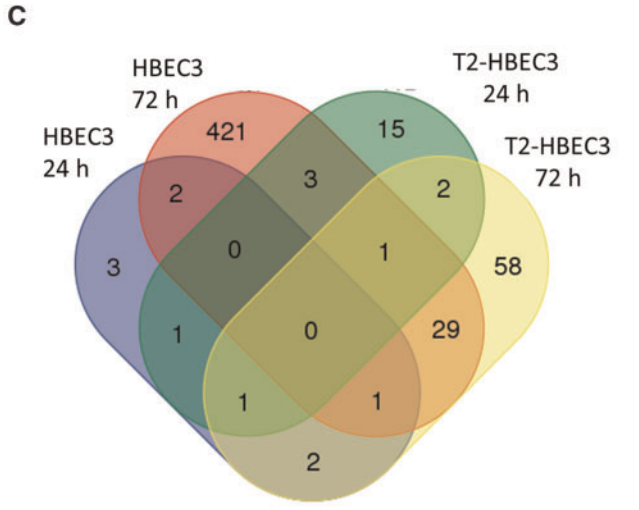

D

	HBEC3			T2-HBEC3	
	24 h	72 h		24 h	72 h
Genes	log2FC	log2FC	Genes	log2FC	log2FC
RNY1	0.58	1.40	SLC29A2	0.59	0.70
LDLR	0.77	1.83	SQLE	1.10	1.67
STOM	-0.68	-0.94	PNP	0.82	0.65
			ABCC3	0.69	1.14

Figure 4. Significantly deregulated genes in the short-term DEP-exposure experiments. A, Venn diagram display statistically significant deregulated genes between HBEC3 and T2-HBEC3 exposed to 50 and 200 µg/ml DEP for 48 h and (C) Venn diagram display statistically significant deregulated genes between HBEC3 and T2-HBEC3 exposed to 200 µg/ml DEP for 24 and 72 h. $p < .001$ and log2FC < -0.58 and > 0.58 (Moderated *t*-statistics). (B) Heat maps display common deregulated genes within each cell line between the 2 exposure concentrations while (D) heat maps display common deregulated genes within each cell line between the 2 time-points. Red and green indicates up- and downregulation of gene expression, respectively.

investigating the effects of not only DEP-extracts, but also of intact particles with all its constituents.

All DEP-transformed clones showed significantly reduced *CDH1* expression, accentuating the importance of E-cadherin downregulation in EMT. With the exception of clone No. 3, the clones showed increased expression of *CDH2* and *VIM*. Thus, variability in expression of EMT-marker genes between the transformed clones was found. EMT is a plastic process and cancer cells of epithelial origin may pass through EMT to various extent, where some cells may retain particular epithelial traits, whereas others may become fully mesenchymal (Kalluri and Weinberg, 2009). The present data underline that clones with different patterns of expression of EMT-marker genes can have the capacity to grow anchorage-independently in soft agar.

Significantly increased expression of *TWIST1*, *ZEB1*, and *SNAI2* was only measured in T2-HBEC3. T2-HBEC3 also displayed the highest increase in vimentin, compared with the other clones. Vimentin is important in cytoskeleton organization and cellular mechanical strength in cancers of epithelial origin. Thus, induction of vimentin may have contributed to the change towards a mesenchymal/fibroblast-like morphology (Liu *et al.*, 2015). T2-HBEC3 showed reduced migration compared with HBEC3. Generally, increased cellular capacity to migrate and invade coincides with EMT. However, altered migration and

invasive potential may be uncoupled events in EMT (Schaeffer *et al.*, 2014). It was shown that exposure to DEP-induced disruption of cell-polarity and focal adhesion remodeling in alveolar epithelial cells leading to disruption of directional migration (LaGier *et al.*, 2013). A recent study also reported reduced migratory potential for CSC-transformed HBEC2 (Bersaas *et al.*, 2016). However, in contrast to CSC-transformed HBEC2, the DEP-transformed T2-HBEC3 did not invade a reconstituted basement membrane, suggesting that these cells represent a model of early steps in carcinogenesis.

Table 2. Significantly Deregulated Pathways in the Short-Term DEP-Exposure Experiments

Deregulated Pathways
Common deregulated pathways[a]
Tryptophan metabolism
Valine, leucine and isoleucine degradation
Terpenoid backbone biosynthesis
Steroid biosynthesis
Deregulated pathways in HBEC3[b]
Metabolism of xenobiotics by cytochrome P450
Phagosome
Aldosterone-regulated sodium reabsorption
Deregulated pathways in T2-HBEC3[c]
Synthesis and degradation of ketone bodies
Malaria
Butanoate metabolism
Rheumatoid arthritis
Pyruvate metabolism
Graft-versus-host disease
Rheumatoid arthritis

Data are from the dose-response and time-course experiments combined. Pathways have adjusted p-value (Holm) $< .01$.
[a]Pathways (Goemans's global test and the KEGG database) deregulated in both HBEC3 and T2-HBEC3.
[b]Pathways deregulated in HBEC3 only.
[c]Pathways deregulated in T2-HBEC3 only.

Results from baseline gene expression profiling revealed deregulation of several pathways in T2-HBEC3 related to carcinogenesis. Originally identified as guidance for axons during central nervous system development, molecules belonging to semaphorins and ephrins are now appreciated as contributors in lung carcinogenesis (Nasarre *et al.*, 2010). Alterations in integrins and structural constituents of extracellular matrix may participate in altering proliferative, migratory and apoptotic signals mediated by ie, phosphatidylinositol 3-kinase and MAPK (Paoli *et al.*, 2013). These pathways together with mTOR are frequently deregulated in lung carcinogenesis through alterations in genes coding for key components of the cascades or cell-surface receptors (De *et al.*, 2012; Ekman *et al.*, 2012).

Gene expression profiling from short-term DEP-exposures revealed deregulation of *"Tryptophan metabolism"*, *"Valine, leucine and isoleucine degradation"*, *"Terpenoid backbone biosynthesis"*, and *"Steroid biosynthesis"* pathways in both HBEC3 and T2-HBEC3. In addition, DEP specifically induced deregulation of pathways related to particle uptake and xenobiotic metabolism in HBEC3, whereas pathways related to inflammation and metabolism were affected in T2-HBEC3. Microarray analysis of A549 exposed to Milan urban air winter $PM_{2.5}$ revealed deregulated pathways involved in ie, xenobiotic metabolism, inflammation and lipid metabolism, while summer $PM_{2.5}$ preferentially affected pathways involved in cell signaling, -function, and -assembly (Gualtieri *et al.*, 2012). In BEAS-2B, Milan urban PM showed regulation of

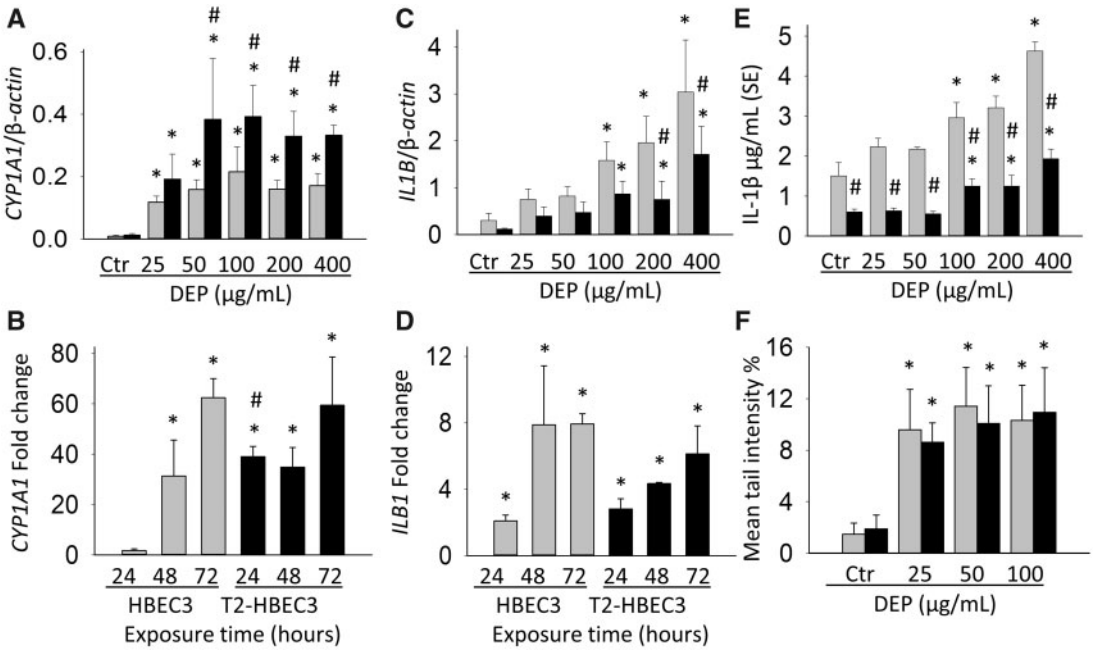

Figure 5. Gene expression of *CYP1A1* and *IL1B*, and analysis of DNA strand breaks by Comet assay. HBEC3 in gray bars and T2-HBEC3 in black bars. Gene expression of *CYP1A1* (A) and *IL1B* (C) in HBEC3 and T2-HBEC3 from the 48 h dose-response experiment and *CYP1A1* (B) and *IL1B* (D) from the time-course experiment with 200 μg DEP/mL. Gene expression levels for the dose-response experiment (Figs. 5A and 5C) were measured by RT-qPCR and normalized to *β-actin* ($2^{-\Delta\Delta Cq}$) (mean ± SD, $n = 3$). For the time-course experiment (Figs. 5B and 5D), gene expression levels were normalized to *β-actin* and the corresponding unexposed control at the given time-point. E, Protein levels of IL-1β release to cell culture media from HBEC3 and T2-HBEC3 were measured by ELISA in the dose-response experiment. * and #: $p < .05$ (linear mixed effects model). *Statistically significant differences between control to concentration/time DEP. #Statistically significant differences between HBEC3 and T2-HBEC3 at corresponding exposure concentrations/time. F, DNA strand breaks were measured by alkali Comet assay in a dose-response experiment with HBEC3 and T2-HBEC3. Data display mean % tail DNA ± SD, $n = 3$. *$p < .05$ (Log-transformed data, ANOVA Dunnett's post hoc test).

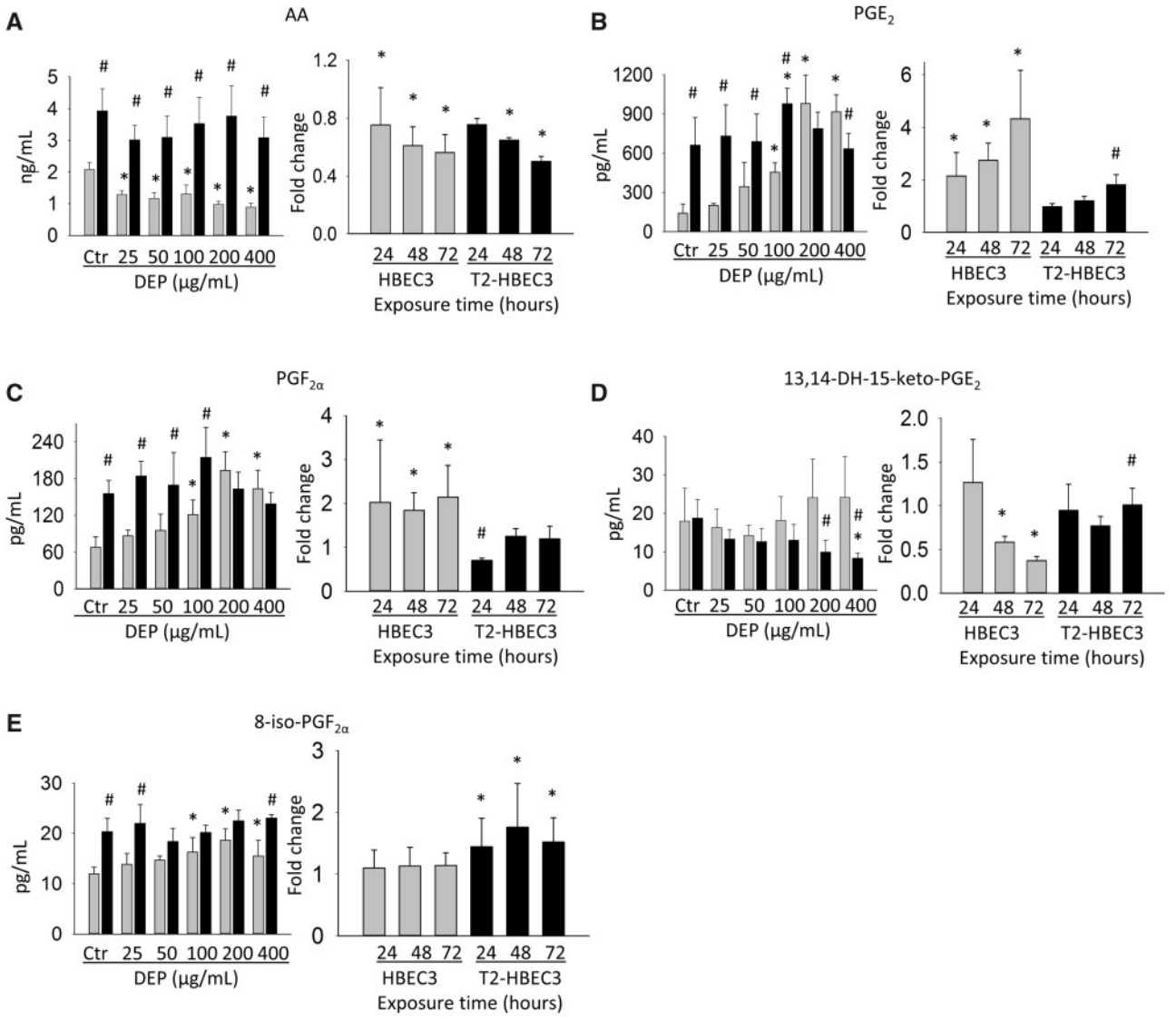

Figure 6. Release of AA and PGs to cell culture media in the short-term DEP-exposure experiments. HBEC3 in gray bars and T2-HBEC3 in black bars. (A) AA, (B) PGE_2, (C) $PGF_{2\alpha}$, (D) 13, 14-DH-15-keto-PGE_2, (E) 8-iso-$PGF_{2\alpha}$. Data display mean ± SD, $n = 3$. Eicosanoid concentration measured from the dose-response experiment is presented in pg/ml or ng/ml, while those from the time-course experiment are presented as fold change compared with the corresponding unexposed control at the given time-point. * and #: $p < .05$ (linear mixed effects model). *Statistically significant differences between control to concentration DEP and between control to exposure time. #Statistically significant differences between HBEC3 and T2-HBEC3 at corresponding exposure concentrations and at corresponding time-points.

pathways involved in oxidative stress, inflammation and DNA-damage responses (Longhin *et al.*, 2016). Thus, exposure to DEP and urban PM with different particle and chemical characteristics appears to elicit deregulation of several similar pathways.

Microarray analysis of BEAS-2B exposed to DEP and biodiesel particle extracts also showed deregulation of *"Metabolism of xenobiotics by cytochrome p450"*, *"Metabolism of lipids and lipoproteins"*, and *"Steroid biosynthesis"*, in addition to other pathways, ie, related to bile acid synthesis (Libalova *et al.*, 2016). Most deregulated pathways may be linked to aryl hydrocarbon receptor (AHR) signaling and probably be explained by differences in particle PAH levels (Gualtieri *et al.*, 2012). Accordingly, PAH was reported to be central for the toxic effects of SRM1649a extracts, via its AHR dependent mutagenic and non-genotoxic effects (Andrysik *et al.*, 2011).

Associations between the tryptophan metabolite kynurenine, inflammation and cancer have been suggested (Opitz *et al.*, 2011). Degradation of valine, leucine, and isoleucine generates propionyl-CoA and/or acetyl-CoA utilizable for lipid synthesis. Lung lipid homeostasis is a tightly regulated process and its disruption can cause inflammation participating in lung injury (Plantier *et al.*, 2012). The *"Mevalonate (MVA) pathway"* generates isoprenoids, being key metabolites for *de novo* cholesterol and steroid synthesis (Goldstein and Brown, 1990). A link between inflammation, carcinogenesis and the MVA pathway has been reported (Karlic *et al.*, 2015; Steffens and Mach, 2004). Dysregulation of small GTPases of the Ras family is important in carcinogenesis, and their activation depends on the addition of isoprenyl (Konstantinopoulos *et al.*, 2007). Regulation of *"Terpenoid backbone biosynthesis"* may represent a mechanism for altered posttranscriptional modification of such proteins. *"Steroid biosynthesis"* is linked to the MVA pathway and emerging evidence from both epidemiological and experimental studies indicate correlations with

steroid hormones and human nonsmall-cell lung cancer progression (Kazmi *et al.*, 2012). Together, deregulation of these pathways may participate as "routes of action" for detrimental effects of DEP.

Short-term exposure to DEP induced expression *CYP1A1* and *CYP1B1* (RT-qPCR) in both HBEC3 and T2-HBEC3 despite low content of organic carbon compounds in SRM2975. Metabolic activation of PAH by the cytochrome P450 family can lead to early initiating events in carcinogenesis (Shimada and Fujii-Kuriyama, 2004), and *CYP1A1* may constitute a sensitive biomarker for DEP-induced effects (Totlandsdal *et al.*, 2010). Higher induction of *CYP1A1* was found in T2-HBEC3 compared with HBEC3. *CYP1A1* was also induced at an earlier time-point in T2-HBEC3, indicating a greater xenobiotic response to DEP in the transformed cells. *CYP1B1* followed a similar pattern. Significantly higher levels of *IL1A* and *IL1B* gene expression, and IL-1β secretion were measured from HBEC3 compared with T2-HBEC3 after DEP-exposure. IL-1β is critical for DEP-induced pulmonary inflammation (Provoost *et al.*, 2011). In accordance with earlier findings (Arlt *et al.*, 2015; Totlandsdal *et al.*, 2010), our data support an inverse relationship between induction of CYP-enzymes and inflammation. Combined, this may indicate a downregulation of inflammatory responses in T2-HBEC3 that could represent a way to increase cell survival after DEP-exposure.

Increased single strand breaks/alkaline-labile sites were observed after DEP-exposure, while oxidative DNA-damage was unchanged. Similar results were found in BEAS-2B exposed to Milan winter $PM_{2.5}$ (Gualtieri *et al.*, 2011). In contrast, exposure of A549 to SRM2975 increased oxidative DNA-damage (Jantzen *et al.*, 2012). This discrepancy may be related to experimental setup, including intrinsic differences between cell lines. Accordingly, lack of induction of oxidative DNA-damage by SRM1650b extract was also reported in liver, pulmonary, and prostate cell lines (Pálková *et al.*, 2015), suggesting that increased formation of reactive oxygen species (ROS) may not always contribute to DEP-induced DNA-damage.

Higher secretion of AA from T2-HBEC3 may be linked to induction of genes belonging to the phospholipase A2 family (Supplementary Table 2). PGE_2 and $PGF_{2\alpha}$, the major secreted AA metabolites, increased dose-dependently for HBEC3, whereas generally higher and unchanged levels were measured for T2-HBEC3. Similar results were obtained from the time-course experiment where higher levels of PGE_2 and $PGF_{2\alpha}$ release after DEP-exposure were observed for HBEC3. The generally higher *PTGES* (PG E synthase, Supplementary Figure 2E) and PGE_2 levels, in addition to reduced E-cadherin found in T2-HBEC3, are in compliance with previous results showing inverse association between decreased E-cadherin levels and increased PGE_2 synthesis (Brouxhon *et al.*, 2007). DEP-induced PGE_2 and $PGF_{2\alpha}$ secretion has been reported from canine AM and in bronchoalveolar lavage fluid (BALF) from mouse and rat (Alessandrini *et al.*, 2009; Beck-Speier *et al.*, 2005; Henderson *et al.*, 1988). Higher baseline levels of *COX-2* were measured in T2-HBEC3, which may aid in explaining increased secretion of several eicosanoids. Interestingly, no dose-response relationship of *COX-2* induction was found following DEP-exposure for either cell line. However, a significant increase with time was found for HBEC3 (Supplementary Figure 2D).

Levels of 8-iso-$PGF_{2\alpha}$ increased dose-dependently in HBEC3 indicating increased lipid peroxidation. Secretion of 8-iso-$PGF_{2\alpha}$ increased with time in T2-HBEC3. Generally higher levels of 8-iso-$PGF_{2\alpha}$ measured in T2-HBEC3 after DEP-exposure indicates continuous lipid peroxidation; a trait commonly found in cancer cells showing increased ROS production (Toyokuni *et al.*, 1995). Generation of 8-iso-$PGF_{2\alpha}$ after DEP-exposure has been found in canine AM and BALF from mouse (Alessandrini *et al.*, 2009; Beck-Speier *et al.*, 2005). Combined, these data indicate that HBEC3 elicits a greater inflammatory response to short-term DEP-exposure meanwhile T2-HBEC3 is constitutively sensitized, thus, potentially having implications for DEP-induced inflammation and carcinogenesis.

Results indicated cellular uptake of DEP mainly concentrated around the cell nucleus, but particle agglomerates attached to the cell surface were also found. Uptake in epithelial cells may be mediated by actin-dependent phagocytosis (Boland *et al.*, 1999), which by itself can trigger biological responses. However, particles and/or adsorbed organic chemicals may also interact directly with cellular plasma membranes and elicit biological responses through ion channels and membrane and intracellular receptors (Øvrevik *et al.*, 2015).

SRM2975 represents a well characterized and widely used particle model of DEP (Klein *et al.*, 2017). Interestingly, these particles with a low concentration of organic compounds (approximately 2%), nevertheless induced transformation. As exposures to DEP in occupational settings can be considerable, the concentration used in the transformation study (100 μg/ml) may be considered biologically relevant (Benbrahim-Tallaa *et al.*, 2012; Li *et al.*, 2003). Also, this concentration has frequently been used in other mechanistic studies (Beck-Speier *et al.*, 2005; Jantzen *et al.*, 2012).

In conclusion, long-term DEP-exposure transformed HBEC3 *in vitro*. T2-HBEC3 acquired several early traits of carcinogenesis. Furthermore, HBEC3 and T2-HBEC3 show different baseline gene expression profiles and susceptibility to short-term DEP-exposure regarding genes involved in xenobiotic and lipid metabolism, as well as inflammation. This study adds information of immunomodulatory effect markers measured from DEP-exposure and differences between normal and sensitized bronchial epithelial cells of the human lung.

SUPPLEMENTARY DATA

Supplementary data are available at *Toxicological Sciences* online.

ACKNOWLEDGMENTS

The authors wish to thank Ms Rita Bæra for skillful technical assistance.

FUNDING

This study was supported by the Czech Science Foundation (grant No. 14-22016S to J.N., E.H., and M.M.; P503-12-G147 to K.V. and H.L.) and by the Ministry of Youth, Education and Sports of the Czech Republic (LO1508 to P.R. and. LM2015073 to J.T.).

REFERENCES

Alessandrini, F., Beck-Speier, I., Krappmann, D., Weichenmeier, I., Takenaka, S., Karg, E., Kloo, B., Schulz, H., Jakob, T., Mempel, M., *et al.* (2009). Role of oxidative stress in ultrafine particle-induced exacerbation of allergic lung inflammation. *Am. J. Respir. Crit. Care Med.* **179**, 984–991.

Andrysík, Z., Vondráček, J., Marvanová, S., Ciganek, M., Neča, J., Pěnčíková, K., Mahadevan, B., Topinka, J., Baird, W. M.,

Kozubík, A., *et al.* (2011). Activation of the aryl hydrocarbon receptor is the major toxic mode of action of an organic extract of a reference urban dust particulate matter mixture: The role of polycyclic aromatic hydrocarbons. *Mutat. Res.* **714**, 53–62.

Arlt, V. M., Krais, A. M., Godschalk, R. W., Riffo-Vasquez, Y., Mrizova, I., Roufosse, C. A., Corbin, C., Shi, Q., Frei, E., Stiborova, M., *et al.* (2015). Pulmonary Inflammation Impacts on CYP1A1-Mediated Respiratory Tract DNA Damage Induced by the Carcinogenic Air Pollutant Benzo[a]pyrene. *Toxicol. Sci.* **146**, 213–225.

Bals, R., and Hiemstra, P. S. (2004). Innate immunity in the lung: How epithelial cells fight against respiratory pathogens. *Eur. Respir. J.* **23**, 327–333.

Beck-Speier, I., Dayal, N., Karg, E., Maier, K. L., Schumann, G., Schulz, H., Semmler, M., Takenaka, S., Stettmaier, K., Bors, W., *et al.* (2005). Oxidative stress and lipid mediators induced in alveolar macrophages by ultrafine particles. *Free Radic. Biol. Med.* **38**, 1080–1092.

Benbrahim-Tallaa, L., Baan, R. A., Grosse, Y., Lauby-Secretan, B., El Ghissassi, F., Bouvard, V., Guha, N., Loomis, D., and Straif, K. (2012). Carcinogenicity of diesel-engine and gasoline-engine exhausts and some nitroarenes. *Lancet Oncol.* **13**, 663–664.

Bersaas, A., Arnoldussen, Y. J., Sjoberg, M., Haugen, A., and Mollerup, S. (2016). Epithelial-mesenchymal transition and FOXA genes during tobacco smoke carcinogen induced transformation of human bronchial epithelial cells. *Toxicol. In Vitro* **35**, 55–65.

Bhavaraju, L., Shannahan, J., William, A., McCormick, R., McGee, J., Kodavanti, U., and Madden, M. (2014). Diesel and biodiesel exhaust particle effects on rat alveolar macrophages with in vitro exposure. *Chemosphere* **104**, 126–133.

Boland, S., Baeza-Squiban, A., Fournier, T., Houcine, O., Gendron, M. C., Chevrier, M., Jouvenot, G., Coste, A., Aubier, M., and Marano, F. (1999). Diesel exhaust particles are taken up by human airway epithelial cells in vitro and alter cytokine production. *Am. J. Physiol.* **276**, L604–L613.

Brouxhon, S., Kyrkanides, S., O'Banion, M. K., Johnson, R., Pearce, D. A., Centola, G. M., Miller, J. N., McGrath, K. H., Erdle, B., Scott, G., *et al.* (2007). Sequential down-regulation of E-cadherin with squamous cell carcinoma progression: Loss of E-cadherin via a prostaglandin E2-EP2 dependent posttranslational mechanism. *Cancer Res.* **67**, 7654–7664.

Cassee, F. R., Heroux, M. E., Gerlofs-Nijland, M. E., and Kelly, F. J. (2013). Particulate matter beyond mass: Recent health evidence on the role of fractions, chemical constituents and sources of emission. *Inhal. Toxicol.* **25**, 802–812.

Cohen, A. J., Ross, A. H., Ostro, B., Pandey, K. D., Krzyzanowski, M., Kunzli, N., Gutschmidt, K., Pope, A., Romieu, I., Samet, J. M., *et al.* (2005). The global burden of disease due to outdoor air pollution. *J. Toxicol. Environ. Health A* **68**, 1301–1307.

Damiani, L. A., Yingling, C. M., Leng, S., Romo, P. E., Nakamura, J., and Belinsky, S. A. (2008). Carcinogen-induced gene promoter hypermethylation is mediated by DNMT1 and causal for transformation of immortalized bronchial epithelial cells. *Cancer Res.* **68**, 9005–9014.

De, L. A., Maiello, M. R., D'Alessio, A., Pergameno, M., and Normanno, N. (2012). The RAS/RAF/MEK/ERK and the PI3K/AKT signalling pathways: Role in cancer pathogenesis and implications for therapeutic approaches. *Expert. Opin. Ther. Targets* **16**, S17–S27.

Delgado, O., Kaisani, A. A., Spinola, M., Xie, X. J., Batten, K. G., Minna, J. D., Wright, W. E., and Shay, J. W. (2011). Multipotent capacity of immortalized human bronchial epithelial cells. *PLoS One* **6**, e22023.

Du, P., Kibbe, W. A., and Lin, S. M. (2008). lumi: A pipeline for processing Illumina microarray. *Bioinformatics* **24**, 1547–1548.

Ekman, S., Wynes, M. W., and Hirsch, F. R. (2012). The mTOR pathway in lung cancer and implications for therapy and biomarker analysis. *J. Thorac. Oncol.* **7**, 947–953.

Ensell, M. X., Whong, W. Z., Heng, Z. C., Nath, J., and Ong, T. (1998). In vitro and in vivo transformation in rat tracheal epithelial cells exposed to diesel emission particles and related compounds. *Mutat. Res.* **412**, 283–291.

Gazdar, A. F., Gao, B., and Minna, J. D. (2010). Lung cancer cell lines: Useless artifacts or invaluable tools for medical science? *Lung Cancer* **68**, 309–318.

Goldstein, J. L., and Brown, M. S. (1990). Regulation of the mevalonate pathway. *Nature* **343**, 425–430.

Gualtieri, M., Longhin, E., Mattioli, M., Mantecca, P., Tinaglia, V., Mangano, E., Proverbio, M. C., Bestetti, G., Camatini, M., and Battaglia, C. (2012). Gene expression profiling of A549 cells exposed to Milan PM2.5. *Toxicol. Lett* **209**, 136–145.

Gualtieri, M., Ovrevik, J., Mollerup, S., Asare, N., Longhin, E., Dahlman, H. J., Camatini, M., and Holme, J. A. (2011). Airborne urban particles (Milan winter-PM2.5) cause mitotic arrest and cell death: Effects on DNA, mitochondria, AhR binding and spindle organization. *Mutat. Res.* **713**, 18–31.

Gutzkow, K. B., Langleite, T. M., Meier, S., Graupner, A., Collins, A. R., and Brunborg, G. (2013). High-throughput comet assay using 96 minigels. *Mutagenesis* **28**, 333–340.

Hasegawa, M. M., Nishi, Y., Tsuda, H., Inui, N., and Morimoto, K. (1988). Effects of diesel exhaust particles on chromosome aberration, sister chromatid exchange and morphological transformation in cultured mammalian cells. *Cancer Lett.* **42**, 61–66.

HEI Diesel Epidemiology Panel. 2015. *Diesel Emissions and Lung Cancer: An Evaluation of Recent Epidemiological Evidence for Quantitative Risk Assessment. Special Report 19*.Boston, MA: Health Effects Institute

Henderson, R. F., Leung, H. W., Harmsen, A. G., and McClellan, R. O. (1988). Species differences in release of arachidonate metabolites in response to inhaled diluted diesel exhaust. *Toxicol. Lett.* **42**, 325–332.

Jantzen, K., Roursgaard, M., Desler, C., Loft, S., Rasmussen, L. J., and Moller, P. (2012). Oxidative damage to DNA by diesel exhaust particle exposure in co-cultures of human lung epithelial cells and macrophages. *Mutagenesis* **27**, 693–701.

Kalluri, R., and Weinberg, R. A. (2009). The basics of epithelial-mesenchymal transition. *J. Clin. Invest.* **119**, 1420–1428.

Karlic, H., Thaler, R., Gerner, C., Grunt, T., Proestling, K., Haider, F., and Varga, F. (2015). Inhibition of the mevalonate pathway affects epigenetic regulation in cancer cells. *Cancer Genet.* **208**, 241–252.

Kazmi, N., Márquez-Garbán, D. C., Aivazyan, L., Hamilton, N., Garon, E. B., Goodglick, L., and Pietras, R. J. M.-G. D. A. L. e. a. (2012). The role of estrogen, progesterone and aromatase in human non-small-cell lung cancer. *Lung Cancer Manag.* **1**, 259–272.

Klein, S. G., Cambier, S., Hennen, J., Legay, S., Serchi, T., Nelissen, I., Chary, A., Moschini, E., Krein, A., Blömeke, B., *et al.* (2017). Endothelial responses of the alveolar barrier in vitro in a dose-controlled exposure to diesel exhaust particulate matter. *Part Fibre Toxicol.* **14**, 7.

Konstantinopoulos, P. A., Karamouzis, M. V., and Papavassiliou, A. G. (2007). Post-translational modifications and regulation

of the RAS superfamily of GTPases as anticancer targets. *Nat. Rev. Drug Discov.* **6**, 541–555.

LaGier, A. J., Manzo, N. D., and Dye, J. A. (2013). Diesel exhaust particles induce aberrant alveolar epithelial directed cell movement by disruption of polarity mechanisms. *J. Toxicol. Environ. Health A* **76**, 71–85.

Lamouille, S., Xu, J., and Derynck, R. (2014). Molecular mechanisms of epithelial-mesenchymal transition. *Nat. Rev. Mol. Cell Biol.* **15**, 178–196.

Li, N., Hao, M., Phalen, R. F., Hinds, W. C., and Nel, A. E. (2003). Particulate air pollutants and asthma. A paradigm for the role of oxidative stress in PM-induced adverse health effects. *Clin. Immunol.* **109**, 250–265.

Libalova, H., Rossner, P., Vrbova, K., Brzicova, T., Sikorova, J., Vojtisek-Lom, M., Beranek, V., Klema, J., Ciganek, M., Neca, J., *et al.* (2016). Comparative Analysis of Toxic Responses of Organic Extracts from Diesel and Selected Alternative Fuels Engine Emissions in Human Lung BEAS-2B Cells. *Int. J. Mol. Sci.* **17**, 1833.

Liu, C. Y., Lin, H. H., Tang, M. J., and Wang, Y. K. (2015). Vimentin contributes to epithelial-mesenchymal transition cancer cell mechanics by mediating cytoskeletal organization and focal adhesion maturation. *Oncotarget* **6**, 15966–15983.

Longhin, E., Capasso, L., Battaglia, C., Proverbio, M. C., Cosentino, C., Cifola, I., Mangano, E., Camatini, M., and Gualtieri, M. (2016). Integrative transcriptomic and protein analysis of human bronchial BEAS-2B exposed to seasonal urban particulate matter. *Environ. Pollut.* **209**, 87–98.

Menter, D. G., and Dubois, R. N. (2012). Prostaglandins in cancer cell adhesion, migration, and invasion. *Int. J. Cell Biol.* **2012**, 723419.

Morrow, J. D., Hill, K. E., Burk, R. F., Nammour, T. M., Badr, K. F., and Roberts, L. J. (1990). A series of prostaglandin F2-like compounds are produced in vivo in humans by a non-cyclooxygenase, free radical-catalyzed mechanism. *Proc. Natl. Acad. Sci U. S. A.* **87**, 9383–9387.

Nasarre, P., Potiron, V., Drabkin, H., and Roche, J. l. (2010). Guidance molecules in lung cancer. *Cell Adhes. Migr.* **4**, 130–145.

Olsen, A. K., Duale, N., Bjoras, M., Larsen, C. T., Wiger, R., Holme, J. A., Seeberg, E. C., and Brunborg, G. (2003). Limited repair of 8-hydroxy-7, 8-dihydroguanine residues in human testicular cells. *Nucleic Acids Res.* **31**, 1351–1363.

Opitz, C. A., Litzenburger, U. M., Sahm, F., Ott, M., Tritschler, I., Trump, S., Schumacher, T., Jestaedt, L., Schrenk, D., Weller, M., *et al.* (2011). An endogenous tumour-promoting ligand of the human aryl hydrocarbon receptor. *Nature* **478**, 197–203.

Øvrevik, J., Refsnes, M., Låg, M., Holme, J. A., and Schwarze, P. E. (2015). Activation of proinflammatory responses in cells of the airway mucosa by particulate matter: Oxidant- and non-oxidant-mediated triggering mechanisms. *Biomolecules* **5**, 1399–1440.

Pálková, L., Vondráček, J., Trilecová, L., Ciganek, M., Pěnčíková, K., Neča, J., Milcová, A., Topinka, J., and Machala, M. (2015). The aryl hydrocarbon receptor-mediated and genotoxic effects of fractionated extract of standard reference diesel exhaust particle material in pulmonary, liver and prostate cells. *Toxicol. In Vitro* **29**, 438–448.

Pallier, K., Cessot, A., Cote, J. F., Just, P. A., Cazes, A., Fabre, E., Danel, C., Riquet, M., Devouassoux-Shisheboran, M., Ansieau, S., *et al.* (2012). TWIST1 a new determinant of epithelial to mesenchymal transition in EGFR mutated lung adenocarcinoma. *PLoS. One* **7**, e29954.

Paoli, P., Giannoni, E., and Chiarugi, P. (2013). Anoikis molecular pathways and its role in cancer progression. *Biochim. Biophys. Acta* **1833**, 3481–3498.

Peinado, H., Olmeda, D., and Cano, A. (2007). Snail, Zeb and bHLH factors in tumour progression: An alliance against the epithelial phenotype? *Nat. Rev. Cancer* **7**, 415–428.

Plantier, L., Besnard, V., Xu, Y., Ikegami, M., Wert, S. E., Hunt, A. N., Postle, A. D., and Whitsett, J. A. (2012). Activation of sterol-response element-binding proteins (SREBP) in alveolar type II cells enhances lipogenesis causing pulmonary lipotoxicity. *J. Biol. Chem.* **287**, 10099–10114.

Pope, C. A., III, Burnett, R. T., Thun, M. J., Calle, E. E., Krewski, D., Ito, K., and Thurston, G. D. (2002). Lung cancer, cardiopulmonary mortality, and long-term exposure to fine particulate air pollution. *JAMA* **287**, 1132–1141.

Provoost, S., Maes, T., Pauwels, N. S., Vanden Berghe, T., Vandenabeele, P., Lambrecht, B. N., Joos, G. F., and Tournoy, K. G. (2011). NLRP3/caspase-1-independent IL-1beta production mediates diesel exhaust particle-induced pulmonary inflammation. *J. Immunol.* **187**, 3331–3337.

Ramirez, R. D., Sheridan, S., Girard, L., Sato, M., Kim, Y., Pollack, J., Peyton, M., Zou, Y., Kurie, J. M., Dimaio, J. M., *et al.* (2004). Immortalization of human bronchial epithelial cells in the absence of viral oncoproteins. *Cancer Res* **64**, 9027–9034.

Schaeffer, D., Somarelli, J. A., Hanna, G., Palmer, G. M., and Garcia-Blanco, M. A. (2014). Cellular migration and invasion uncoupled: Increased migration is not an inexorable consequence of epithelial-to-mesenchymal transition. *Mol. Cell Biol.* **34**, 3486–3499.

Schwarze, P. E., Totlandsdal, A. I., Lag, M., Refsnes, M., Holme, J. A., and Ovrevik, J. (2013). Inflammation-related effects of diesel engine exhaust particles: Studies on lung cells in vitro. *Biomed. Res. Int.* **2013**, 685142

Shimada, T., and Fujii-Kuriyama, Y. (2004). Metabolic activation of polycyclic aromatic hydrocarbons to carcinogens by cytochromes P450 1A1 and 1B1. *Cancer Sci.* **95**, 1–6.

Steffens, S., and Mach, F. (2004). Anti-inflammatory properties of statins. *Semin. Vasc. Med.* **4**, 417–422.

Sydbom, A., Blomberg, A., Parnia, S., Stenfors, N., Sandstrom, T., and Dahlen, S. E. (2001). Health effects of diesel exhaust emissions. *Eur. Respir. J.* **17**, 733–746.

Totlandsdal, A. I., Cassee, F. R., Schwarze, P., Refsnes, M., and Lag, M. (2010). Diesel exhaust particles induce CYP1A1 and pro-inflammatory responses via differential pathways in human bronchial epithelial cells. *Part Fibre Toxicol.* **7**, 41–47.

Toyokuni, S., Okamoto, K., Yodoi, J., and Hiai, H. (1995). Persistent oxidative stress in cancer. *FEBS Lett.* **358**, 1–3.

Vaz, M., Hwang, S. Y., Kagiampakis, I., Phallen, J., Patil, A., O'Hagan, H. M., Murphy, L., Zahnow, C. A., Gabrielson, E., Velculescu, V. E., *et al.* (2017). Chronic cigarette smoke-induced epigenomic changes precede sensitization of bronchial epithelial cells to single-step transformation by KRAS mutations. *Cancer Cell* **32**, 360–376.

Westerholm, R., and Egebäck, K. E. (1994). Exhaust emissions from light- and heavy-duty vehicles: Chemical composition, impact of exhaust after treatment, and fuel parameters. *Environ. Health Perspect.* **102**, 13–23.